

www.acsnano.org

The Role of Dimer Formation in the Nucleation of Superlattice Transformations and Its Impact on Disorder

Isaiah Y. Chen, Jessica Cimada daSilva, Daniel M. Balazs, Michelle A. Smeaton, Lena F. Kourkoutis, Tobias Hanrath, and Paulette Clancy*



Cite This: ACS Nano 2020, 14, 11431–11441



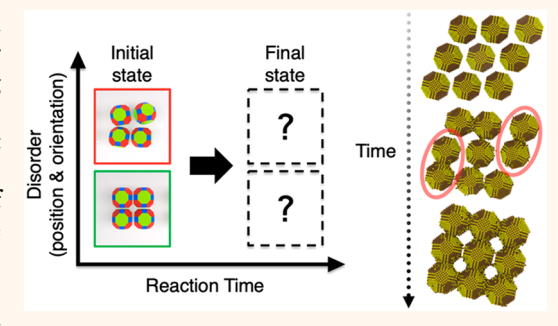
ACCESS I

III Metrics & More

Article Recommendations

Supporting Information

ABSTRACT: The formation of defect-free two-dimensional nanocrystal (NC) superstructures remains a challenge as persistent defects hinder charge delocalization and related device performance. Understanding defect formation is an important step toward developing strategies to mitigate their formation. However, specific mechanisms of defect formation are difficult to determine, as superlattice phase transformations that occur during fabrication are quite complex and there are a variety of factors influencing the disorder in the final structure. Here, we use Molecular Dynamics (MD) and electron microscopy in concert to investigate the nucleation of the epitaxial attachment of lead chalcogenide (PbX, where X = S, Se) NC assemblies. We use an updated implementation



of an existing reactive force field in an MD framework to investigate how initial orientational (mis)alignment of the constituent building blocks impacts the final structure of the epitaxially connected superlattice. This Simple Molecular Reactive Force Field (SMRFF) captures both short-range covalent forces and long-range electrostatic forces and allows us to follow orientational and translational changes of NCs during superlattice transformation. Our simulations reveal how robust the oriented attachment is with regard to the initial configuration of the NCs, measuring its sensitivity to both in-plane and out-of-plane misorientation. We show that oriented attachment nucleates through the initial formation of dimers, which corroborate experimentally observed structures. We present high-resolution structural analysis of dimers at early stages of the superlattice transformation and rationalize their contribution to the formation of defects in the final superlattice. Collectively, the simulations and experiments presented in this paper provide insights into the nucleation of NC oriented attachment, the impact of the initial configuration of NCs on the structural fidelity of the final epitaxially connected superlattice, and the propensity to form commonly observed defects, such as missing bridges and atomic misalignment in the superlattice due to the formation of dimers. We present potential strategies to mitigate the formation of superlattice defects.

KEYWORDS: molecular simulation, reactive force field, atomistic mechanism, nanocrystals, oriented attachment, superlattice, disorder

irecting the assembly of colloidal nanocrystals (NCs) into mesocrystal superstructures presents a grand challenge in nanoscience with significant implications on emerging technologies. Extensive research efforts over the past two decades have resulted in the creation of a broad library of NC building blocks with programmable size, shape, and composition. Among these materials, semiconducting lead chalcogenide NCs, and the epitaxially connected superlattices they can form, present an intriguing experimental system. The electronic structure of these superlattices reflects the balance of strong confinement within the dots and strong coupling between them. Theoretical calculations of these "confined-but-connected" NC solids predict a rich electronic structure with experimentally accessible bandwidths. However, while experimental studies have shown delocalization among a few

coupled dots, ^{2,12,17} it is clear that progress is limited by the present level of disorder within the superlattice. The goal remains to create NC solids whose electronic properties are defined by long-range charge delocalization.

As with other self-assembly processes or mesocrystal formation, the key to producing high-fidelity (large-grain single-crystal superlattice) structures lies in understanding and

Received: May 7, 2020 Accepted: August 17, 2020 Published: August 17, 2020





controlling the initial nucleation stages. Among the reports of various mesocrystal formations, 6,18 the formation of mesocrystals in which constituent building blocks are connected through rigid epitaxial bridges presents a particularly interesting subset. Whereas the bridges enable a long-range atomic-level registry of NCs within their lattice site, the formation of these bridges presents several intriguing, yet unresolved, challenges. Our approach to understand these challenges and optimize the formation of the bridges has been to focus on 2D superlattices as simplified analogues of the 3D mesocrystals. The analogous "crystallization" of 2D polymers has been described as either under thermodynamic or kinetic control. 19-21 The "2D polymerization" of NC superstructures is complicated by the fact that formation of the epitaxial bonds between constituent NC "monomers" is essentially irreversible and sensitive to crystallographic misalignment. The fact that, despite these constraints, epitaxially connected NC solids form with micrometer-sized grains (comprised of $\sim 10^5$ NCs) is astonishing and currently poorly understood.

Disorder inevitably plays a critical role in any experimental self-assembly process. Like snowflakes, no two NCs are identical by virtue of the ensemble variations in NC size, shape, and ligand surface coverage. 22-24 Even in an ideal scenario where individual NCs are identical, the assembly and attachment processes will necessarily involve variations in the position and orientation of the NC building blocks as they come together. Although recent X-ray scattering studies have provided important insights into the interfacial assembly and attachment, 25-27 these measurements reflect an ensemble average in which details are lost concerning the translation and orientation of proximal NCs involved in the attachment. Recent breakthroughs in the development of pixelated detectors optimized for scanning transmission electron microscopy (STEM), such as the electron microscope pixel-array detector (EMPAD), have opened exciting opportunities to capture the position and orientation of each NC. 28,29 This level of detail provides a complete description of the system which goes beyond the precise size and position of each NC to include the degree of in-plane and out-ofplane crystallographic tilt.

Decoupling the relative tolerance to translational and orientational disorder in the epitaxial fusion of proximal NCs (Figure 1) is a challenge that is ideally suited for a molecular simulation approach. Since these parameters cannot be independently controlled in experiments, we systematically analyze this transformation within an *in silico* context. Molecular Dynamics (MD) simulations can provide atomic-scale resolution of structural assembly over time. Essentially, the only input for MD simulations is a suitable "force field", one that represents interatomic/intermolecular interactions suitable for the system of atoms. Critically for this system, we require a force field that provides the ability to capture bond-breaking and bond-forming as the NCs assemble into place.

Several different MD approaches have been used to study the formation of lead chalcogenide superstructures. 30,31 Recent work by Wang *et al.* 11 used MD simulations to study superlattice phase transitions for small 1D structures, focusing on the deformability of PbSe NCs during the phase transition and its impact on disorder. The force field used in that study considered only nonbonded interactions, namely, a short-ranged Lennard-Jones part and a long-ranged Coulombic part. The authors mentioned that this pair potential lacks any description of covalent bonding, which is necessary to model the formation of epitaxial bonds with greater accuracy. To include covalent

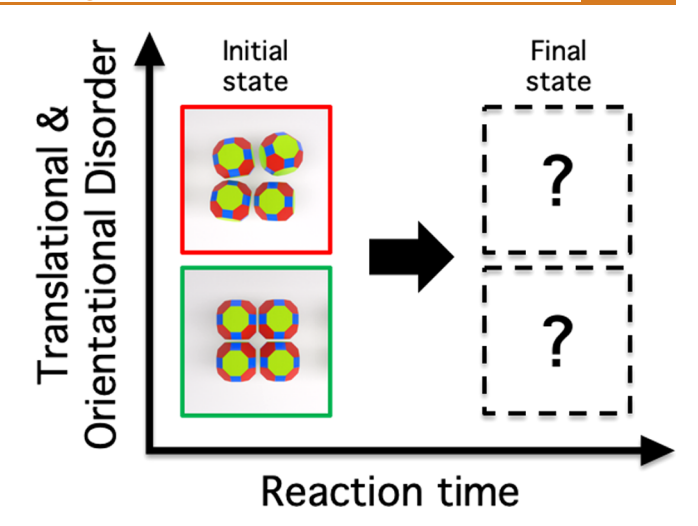


Figure 1. Schematic illustration of the current lack of knowledge of final outcomes for a superlattice as a function of high (red) and low (green) translation and orientational disorder exhibited at early stages of NC self-assembly.

bonding, we use an updated implementation of the Simple Molecular Reactive Force Field (SMRFF),³² which includes long-range electrostatic interactions and short-range covalent bonds to achieve a more accurate description of NC-NC interactions; see the Methods and Supporting Information for more details.

These simulations allow a systematic probe of the influence of the initial configuration of NCs on the final structure of the epitaxially connected superlattice, essentially providing the missing pieces in Figure 1. In this work, we investigated the oriented attachment mechanisms that result in orientational disorder as previously characterized by McCray et al. 13 We simulated different initial configurations in which the translational and orientational order of constituent NCs is varied independently. Some of our initial configurations are idealized perfect structures, but others use initial configurations whose exact positions and orientations have been obtained from advanced electron microscopy and diffraction experiments.² Both the MD simulations and the experiments access molecularscale information (atomic-scale in the case of MD); their close and complementary coupling provides an understanding of the critical role of disorder and dimer formation in the nascent stages of NC attachment. It also uncovers as yet unseen details of the superlattice transformation mechanism, the impact of the initial geometrical configuration of NCs on the final epitaxially connected superlattice, the propensity to form, and the origin of commonly observed superlattice defects. These insights should provide important guidance to future experimental efforts aimed at improving the fidelity of epitaxially connected NC solids.

RESULTS AND DISCUSSION

In this work, we systematically investigated how orientational and translational misalignments in the preassembled superlattice influence the oriented attachment of NCs and lead to the formation of persistent defects. We addressed this question by, first, studying the formation of the smallest structures (dimers and trimers) to understand isolated NC–NC interactions. Then we leveraged high-fidelity structural insights from 4D-STEMgenerated microscopy data to provide realistic starting assemblies from which to investigate the transformation of this array into a superlattice. ²⁹ These assemblies include 16 NCs

Orientation	Ideal	Ordered	Disordered
In-plane	AL SL	AL ∦ SL	AL ∦ SL
Out-of-plane	0°	0-10°	35-45°
Configuration	a	b	С
Initial	3333		
Final	Y A COLOR		
Orientation	Ideal	Ordered	Disordered
In-plane	AL∦ SL	AL∦ SL	AL∦SL
Out-of-plane	0°	0-10°	35-45°
Configuration	d	е	f
Initial	0000	0000	
Final			

Figure 2. Initial and final geometries from MD simulations of 4×4 NC assemblies for six initial configurations. The configurations include both square and hexatic translational arrangements with out-of-plane tilt ranging from 0 to 45° . The reference axes (x and y directions) for all simulations are shown in the final geometry for configuration a.

arranged in hexatic and square structures with various degrees of in-plane and out-of-plane tilt. In our MD simulations, we assume that all NCs are initially identical in size and shape and that all ligands have been stripped from NC surfaces. In practice, there will inevitably be variations in the size and shape of individual NCs. Moreover, ligand coverage is known to be sensitive to the NC facet: whereas {100} facets are effectively bare, ligands remain on the {110} and {111} facets. This study represents progress toward understanding the mechanism of oriented attachment, the robustness of epitaxial bridge formation, and the tendency for superlattice defect formation.

Formation of 1D Structures. First, we investigated epitaxial bridge formation in 1D structures containing two and three NCs, *i.e.*, dimers and trimers initially in a perfectly ordered geometry; see Figure S2, Movie S1 and Movie S2. In both cases, we observe surface reconstruction when the {100} facets of proximal NCs face each other. Surface reconstruction has been commonly observed in *in situ* TEM studies upon ligand desorption and oriented attachment.^{24,31} As NCs move toward each other, atoms at the edges between {111} and {100} facets tend to move toward atoms with opposite charge on the

neighboring NC (as shown in Figure S3). Once four sets of connections at the corners of the {100} facets have been formed, NCs are attracted to each other to complete the formation of the bridge. NCs may rotate in-plane by up to 13° from their original in-plane orientation angle during the oriented attachment process, resulting in orientational misalignment of 5° between the two NCs once the bridge has formed. In the final dimer structure, we observed a small gap defect in the middle of the bridge; the presence of such vacancies in NC–NC bridges have been reported experimentally. NC–NC misalignment emerged in one of the bridges in the trimer structure, similar to an edge dislocation defect, as shown in Figure S2b. These results suggest that even atomically aligned NCs with perfect {100} facet overlap can result in local misalignment.

We also investigated the effect of translational misalignment in the bridge formation process. In dimers with atomically aligned NCs and initial positional offset (5 Å), the NCs undergo rotation in opposite directions to minimize both the potential energy and the positional misalignment in the final structure (Movie S3). These simulations provide a baseline of understanding for epitaxial bridge formation in linear dimers and

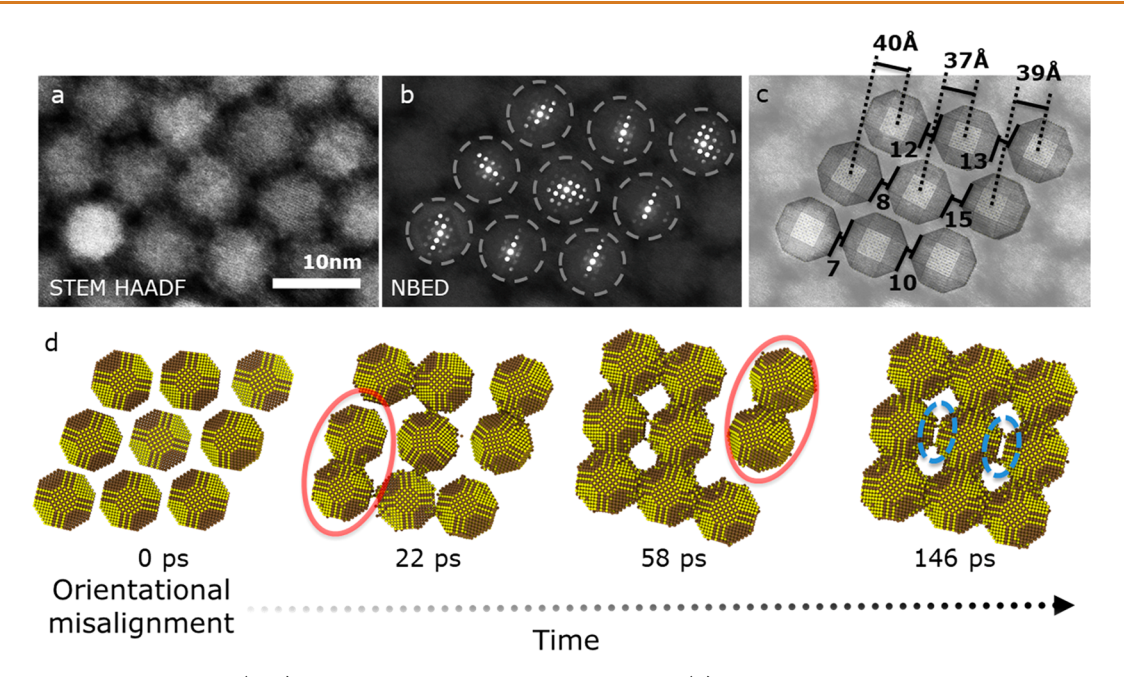


Figure 3. Three experimental images (a-c) of the same hexatic PbS NC superlattice. (d) Time evolution of an MD simulation, starting from the same initial configuration as 3(c). Details: (a) HAADF-STEM image. (b) Nanobeam electron diffraction patterns obtained by 4D-STEM and overlaid with the HAADF image in (a). (c) NC model reconstruction based on NC positions and orientations obtained by 4D-STEM, aligned along the $\langle 11n \rangle_{AL}$ and $\langle 11 \rangle_{SL}$ directions. The added polyhedra are idealized models used to determine NC positions and orientations for use in the MD simulation. The numbers in (c) represent NC separation distances (in Å), and the three distances along the top of the image are offset distances between the centers of the NCs. (d) MD simulation results reveal the formation of dimers (encircled in red) as part of the superlattice transformation and attachment and imperfections in the bridges (encircled by blue dashed lines) which could anneal out given sufficient time.

trimers. Below, we expand the simulations to understand how epitaxial attachment forms in two dimensions.

Effect of Positional and Orientational Disorder on Epitaxial Bridge Formation in 2D Structures. We systematically investigated how the initial configuration affects the final superlattice configuration by varying the translational arrangement and orientation of NCs, shown in Figure 2 (and Movies S4-S9). We investigated two geometric arrangements: square (Figures 2a-c; Movies S4-S6) and hexatic (Figures 2d-f; Movies S7-S9), with three sets of NC orientations for both geometric arrangements: ideal cases (atomically aligned NCs with no out-of-plane tilt; Figure 2a,d), slightly tilted cases (0-10°; Figures 2b,e), and extreme cases in which the NCs were randomly tilted to a large degree (35-45°; Figures 2c,f). Recent structural insights from Cimada daSilva et al.³¹ provided relevant starting configurations to be investigated in our reactive force field MD simulations. At liquid-air interfaces, NCs are constrained to a 2D plane, and the interactions between NCs and the liquid interface affects how the NCs orient and selfassemble into monolayers. Cimada daSilva et al.29 recently reported a crystallographic alignment of analogous PbS NC superlattices that precedes epitaxial attachment for both hexatic and square structures. This study shows that (on average) NCs orient with $\langle 100 \rangle_{AL}$ normal to the interface, 95% of NCs have deviations of <10° from the mean in-plane tilt angle, and 85% of NCs have an absolute out-of-plane tilt angle below 10°. These details were used to inform all the MD simulations here, which increase in realism from more idealized square and hexatic configurations, discussed above, to more realistic hexatic assemblies with experimentally relevant amounts of initial inplane and out-of-plane tilt (as shown in Figure S4 and Figure 3).

The mechanisms of individual bridge formation in 1D and 2D configurations exhibit similar behavior. Qualitatively, compara-

ble NC-NC atomic misalignment defects, such as missing bridges and disordered structures, occur in atomically aligned 1D and 2D structures. Square assemblies with no orientational disorder, or with 0 to 10° of out-of-plane tilt (Figure 2a,b), show the same behavior. The superlattice spacing shrinks uniformly in the plane and bridges start to form as mutually exposed {100} facets between nearest neighbors come within 10 Å of each other. We observe a tendency to form smaller 2D structures during the early stages, which then combine to form the final superlattice. The nearest neighbor in-plane orientational misalignment for these epitaxially attached superlattices is 1.6 \pm 1.1° for Figure 2a and 1.9 \pm 1.3° for Figure 2b. In contrast, NCs with a higher degree of out-of-plane tilt (35-45°) tend to form a completely disordered structure with attachment through {100}, {110}, and {111} facets, and NCs resulting in an out-ofplane orientation ranging from 17 to 45° (as shown in Figure 2c).

For the corresponding hexatic assemblies (Figures 2d-f), we observed an additional orientational and translational movement not seen in the square assemblies. NCs in assemblies with either 0° or 0–10° initial out-of-plane tilt undergo simultaneous in-plane rotation due to forces from neighboring NCs, such that opposing {100} facets align themselves with each other (similar to the 1D case with positionally misaligned NCs, Movie S3). This is consistent with the expected effect of the crystallographic fields of the NCs, which is considered to be a significant driving force in oriented attachment processes. 36,37 Hexatic assemblies of NCs first attach as dimers along the x-axis due to the proximity and alignment of the $\{100\}$ facets along the x-axis along each row. Lateral attachment (i.e., along the y-axis) is not initially possible due to the translational offset of proximal {100} facets. Simultaneously, the 1D structures (and NCs within 1D structures in cases where the irreversible bridge was not yet

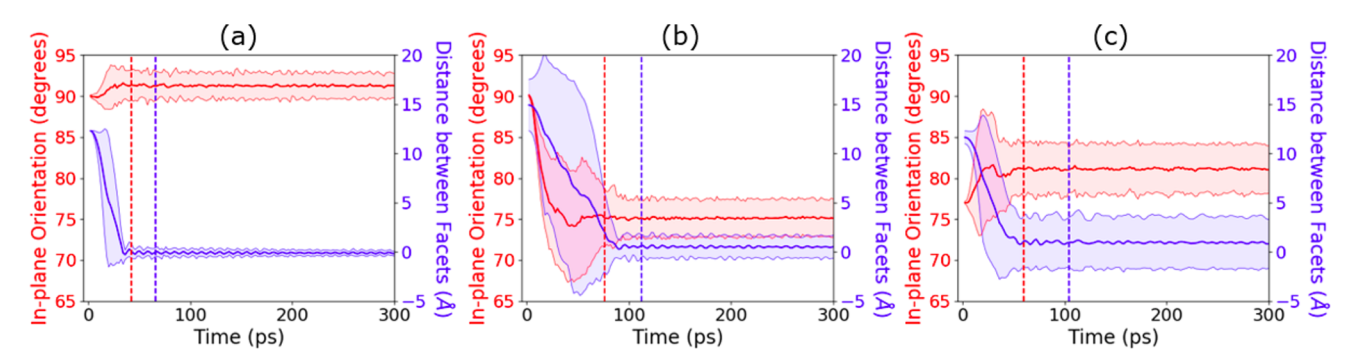


Figure 4. Average in-plane orientation (red) and facet-to-facet distance (blue) for NCs arranged in three different ordered configurations with $0-10^{\circ}$ of initial out-of-plane misalignment: (a) square: Figure 2b; (b) hexatic: Figure 2e; (c) hexatic with added in-plane tilt: Figure S3b. Standard deviations are indicated by the extent of the shaded regions. Vertical red lines represent times where the average in-plane orientation angle has stabilized; blue vertical lines represent times after which there are no more significant positional changes in the assembly.

formed) rotate in the plane. The dimer formation is followed by translation of the 1D structures toward each other to form the final superlattice. The nearest neighbor in-plane orientational misalignment for these epitaxially attached superlattices is $4.1\pm3.8^{\circ}$ for Figure 2d and $2.5\pm1.4^{\circ}$ for Figure 2e. In addition to increased orientational disorder, we also observed increased translational disorder. The resulting superlattice presented a more rhombic-like structure, which is typically observed in epitaxially attached NC superlattices. Lastly, significant angular misalignment in the initial geometry (Figure 2f) leads to a final superlattice with significant disorder in a fashion similar to Figure 2e.

We now investigate the effect of initial in-plane rotation of the NCs by simulating hexatic assemblies with in-plane alignment along the $\langle 11n \rangle_{AL}$ direction (Figure S4); these types of configurations are more closely related to relevant experimental systems that have been observed with 4D-STEM.²⁹ We first show an idealized configuration with no out-of-plane tilt and no variation in in-plane tilt (Figure S4a, Movie S10). Here, we observe the formation of intermediate 2D square superstructures similar to what is observed in the ideal square configuration (see Movie S4 for reference). However, there is an additional translational movement required to achieve a squarelike superlattice, and the final superlattice contains several imperfect bridges. When adding 0-10° of out-of-plane tilt (Figure S4b, Movie S11), the superlattice transformation is dominated by translation of NCs and occurs uniformly through the initial formation of dimers, followed by smaller intermediate 2D structures, before creating the final superlattice. Furthermore, the presence of initial in-plane tilt in this arrangement to have initial alignment along the $\langle 11n \rangle_{AL}$ direction led to the formation of missing epitaxial connections, which is a typical superlattice defect observed in experiments. 13,29 This type of defect occurs because certain pairs of NCs are too far apart and are constrained by other surrounding NCs, preventing the formation of bridges. We note that even if there is no in-plane or out-of-plane misalignment in the initial formation of dimers, the subsequent formation of higher-order oligomers is sensitive to misalignment between the initial dimers. If, instead, we add some slight variation in in-plane tilt $(\pm 5^{\circ})$ to the initial geometry (as shown in the initial frame of Figure S4b), we see that the final structures have similar orientational misalignment (Figure S4c, Movie S12). In this case, we observe a similar dimerization process during the superlattice transformation, and the final geometry contains similar misalignment and missing neck defects. In these assemblies, the nearest-neighbor in-plane

orientational misalignment for the epitaxially attached superlattices is $2.7 \pm 1.9^{\circ}$ for Figure S4a, $3.5 \pm 2.6^{\circ}$ for Figure S4b, and $5.8 \pm 5.7^{\circ}$ for Figure S4c.

Finally, we investigated a similar 3×3 hexatic assembly that precisely reflects the positions and orientations of individual NCs at early stages of the superlattice assembly obtained by 4D-STEM²⁹ (Figure 3). Structural details of the NC superlattice obtained with 4D-STEM present an opportunity to capture specific positions and orientations of polyhedral NCs, as shown in Figure 3. Figure 3a shows a high-angle annular dark-field (HAADF) STEM image of ~7 nm PbS NCs in a hexatic assembly. Figure 3b shows nanobeam electron diffraction (NBED) patterns for single NCs in the assembly recorded using the EMPAD detector.²⁸ This combined information enabled the reconstruction of a NC model shown in Figure 3c. In this model, the $\langle 11n \rangle_{AL}$ direction of the NCs is well aligned along the in-plane $\langle 11 \rangle_{SL}$ direction of the hexatic assembly, and the NCs have an out-of-plane tilt ranging from 0 to 10°. The distinguishing feature of this assembly is the high $\langle 11n \rangle_{AL} ||\langle 11 \rangle_{SL}$ alignment. The formation of such highly aligned superlattices as a precursor to the epitaxially connected structure derives, in part, from the well-defined size and shape distribution of the polyhedral NCs, as well as from the interactions between residual oleate ligands on {11n} facets. 29,38,39 Van der Stam et al. 39 reported that oleic acid ligands on ZnS {101} facets induce atomic alignment in hexagonal 2D superlattices. In 3D superlattices, Novák et al. 38 showed the importance of sitespecific ligand interactions in the formation of body-centered tetragonal PbS superlattices. The concept of ordered selfassembly driven by ligand-ligand interactions to minimize free energy is not unique to superlattices formed at a liquid-air interface but has been long discussed in the context of mesocrystal formation. 18,40

Figure 3d shows snapshots of the time evolution of the 3×3 experimentally derived assembly (Movie S13). NCs aligned inplane along the $\langle 11n \rangle_{AL}$ direction undergo a smaller rotation compared to the previously described hexatic cases (*i.e.*, the final superlattice orientation is determined by that in the initial assembly). The final superlattice is characterized by missing epitaxial connections, similar to what has been observed for the hexatic configurations in Figure S4. During this superlattice transformation, we also observe dimer formation (as marked in Figure 3d). The formation of dimers is intuitive from the perspective of the nucleation of NC-NC attachment in superlattices and is analogous to 2D polymerization processes. ¹⁹

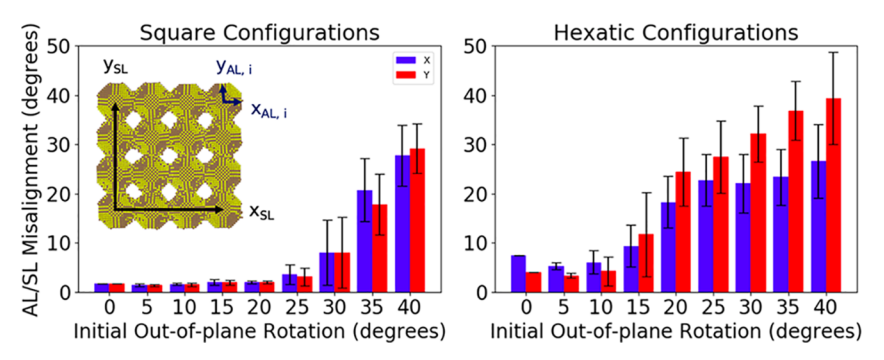


Figure 5. Average local misalignment between the atomic lattices of individual NCs and the overall superlattice. For each rotation angle above 0° , we studied 10 different MD simulations in order to improve the statistics. For each MD simulation, the average misalignment between the atomic lattice and the local superlattice is calculated over 16 NCs along both the x and y axes. The bars show the average values of the 10-run average of AL/SL misalignments for each initial rotation angle. The overlaid geometry is an example of a final superlattice, where we indicate vectors corresponding to the atomic lattice (AL) and superlattice (SL).

atomic lattice alignment and orchestrated translation across multiple NCs, which is less likely to occur. Ondry *et al.*⁴¹ reported detailed pathways for attachment of CdSe NC dimers and described potential effects of imperfect attachment at the NC dimer level. Our simulations take one step further toward the formation of long-range ordered superlattices and reveal more details on the attachment of multiple NCs and the impact dimer formation on superlattice disorder.

MD simulations also allow us to investigate the time evolution of changes in NC orientation and position. Figure 4 shows results for three ordered configurations (Movies S5, S8, and S11), all of which exhibit $0-10^{\circ}$ of misalignment in their initial out-of-plane tilt. We found that changes in angular orientation generally occur within ~50 ps, and changes in position take place within ~100 ps. The criteria used to determine when there are no more significant changes in both translation and rotation were preset thresholds in fluctuations of the values (see the Methods for more details). These results indicate that the superlattice transformation mechanism is initially dominated by rotation of the NCs, followed by translational changes that persist for longer times until all possible bridges in the superlattice are formed. This rapid change in orientation at early stages of the assembly process followed by translation agrees with previous kinetic studies of multilayer PbS selfssembly²⁵ and with monolayer PbS superlattice transformation studies.²⁹ MD timescales and that of the experimental superlattice transformation are different, and comparisons should be interpreted within the context of the relative transformation rates of different configurations in the MD simulations. In experiments, the actual transformation would be much slower due to the presence of solvents and any remaining ligands on the surfaces of the NCs; these factors would most likely retard both the translation and reorientation of the NCs. Standard deviations of inter-NC distances and in-plane orientations can be used as a metric to quantify the extent of disorder. The idealized case in Figure 4a (square) shows much smaller standard deviations than the cases in Figure 4b,c (hexatic), which correspond to up to 10° of initial disorder. The results in Figure 4 suggest that PbS NCs arranged in square (Figure 4a), rather than hexatic (Figure 4b,c) assemblies prior to attachment may be an effective strategy for reducing disorder in the final superlattice. One practical implication of this result is that temporally decoupling NC superlattice transformation and attachment can simplify processing challenges.⁴²

Positional and Orientational Disorder in Initial and Final 2D Geometries. We determined the extent of initial disorder in the preassembled structure that can be tolerated for the system to transform into a large-grain NC solid with minimal defects. We define "defect-free" as implying that each NC is epitaxially connected to its four nearest neighbors in the square assembly. Previous TEM analysis by Whitham et al. 12 showed that, in practice, ~90% of nearest neighbor bridges have formed. To determine this tolerance, we investigated the effect of different amounts of initial out-of-plane rotation, ranging from 0 to 40°, for square and hexatic configurations on the final orientational disorder in the superlattice (similar to the configurations shown in Figure 2). In each simulation, we randomly rotated the NCs to a desired degree of misorientation (0-40°) and calculated the angular misalignment between individual NCs and the local superlattice (Figure 5). Common mechanistic behaviors, such as the formation of 2D intermediate structures, removal of a vacancy in an epitaxial bridge, and dimerization are shown in the Supporting Information (Figures S5-S7).

For initially square configurations, we observed that, once the initial out-of-plane orientation exceeds 25°, the final superlattice exhibits significant persistent misalignment between the atomic lattices and the local superlattice. For hexatic geometries, this threshold is significantly lower; there is much more disorder in the final superlattices, even for initially out-of-plane misorientations of as little as 15°. Square configurations show a similar response to out-of-plane rotation along the major superlattice axes (x and y directions). In contrast, hexatic configurations show an anisotropic response with decreased misalignment along the direction of the initially formed dimers, which is generally in the x-direction, as shown in Figure 5. We attribute this asymmetry to facet overlap along the x-axis within the hexatic assembly. In summary, these simulations show that the transformation of square assemblies is relatively robust to orientational disorder compared to their hexatic counterparts.

The MD simulations provide us with insights into the oriented attachment of NCs: (1) Oriented attachment during superlattice transformation from a hexatic-to-square assembly occurs through the formation of NC dimers and (2) this dimer formation mechanism, in addition to NC orientational disorder in the initial assembly, is the origin of local defects such as NC–NC atomic misalignment and missing bridges. These local defects have been observed by a number of researchers in the field; 13,36,43–46 however, the formation of dimers intrinsic to

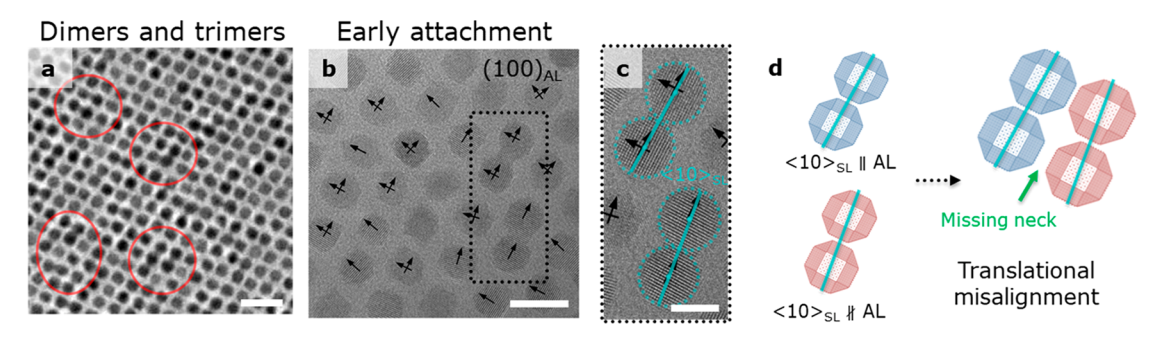


Figure 6. (a) Large field of view TEM image showing dimers and trimers as intermediate structures to a square superlattice. (b) High-resolution TEM image of a monolayer of PbSe NCs assembled on ethylene glycol revealing the in-plane atomic structure of isolated NCs and two dimers in a hexatic assembly and at early stages of oriented attachment. Arrows indicate the $\langle 100 \rangle_{AL}$ direction. (c) Structure of two dimers with parallel and nonparallel NC core-to-core vector and atomic lattice alignment. (d) Illustration of both dimers showing how the misalignment between the atomic lattice and the superlattice results in a missing neck. Scale bars: (a) 20, (b) 10, (c) 5 nm.

self-assembly and attachment experiments has not been previously reported. To validate this computational observation experimentally, we examined the structure of analogous PbSe NC assemblies formed *via* a slow ligand removal strategy by tracking the early stages of superlattice transformation on the subphase (see the Methods for more details).

Figure 6a shows a large field-of-view TEM image obtained 20 min after NC injection on ethylene glycol. Notably, this image captures the nascent stages of epitaxial bridge formation with several dimers and trimers visible. This result is consistent with corresponding stages of the transformation observed in our MD simulations and provides experimental confirmation that the formation of dimers are not rare events; rather, they are an integral part of the oriented attachment mechanism. A highresolution TEM image of two dimers is shown in Figures 6b,c and confirms the existence of an epitaxial attachment in dimer structures. The dimerization can be interpreted in the context of a steadily decreasing ligand coverage on {100} facets. The discrete distribution of the number of ligands means that there will be bare (ligand-free) facets even early in the process. As average NC ligand coverage decreases, the probability increases that two proximate and bare {100} facets will face each other, making attachment more likely. Importantly, the crystal lattices of the two monomers must precisely align to enable formation of a defect-free epitaxial bridge.³³ Ondry et al. reported that NC dimer formation is tolerant to a degree of atomic lattice misalignment, resulting in dislocation defects in the bridge, 41,46 which corroborates our simulation results. As the superlattice transformation and attachment proceeds, the number of dimers and trimers in the superlattice increases, similar to observations in 2D polymerization and percolation studies. 19,47

All NCs with identifiable in-plane orientation shown in Figure 6b are preferentially oriented along the same direction, indicating that dimer formation does not disrupt the overall atomic lattice alignment of NCs in the superlattice. This provides experimental evidence that NCs are, indeed, prealigned at the early stage of the superlattice transformation, in agreement with previously reported results. ^{29,33} Despite NCs within the dimers having well-aligned atomic lattices, in one of the dimers, the NCs' $\langle 100 \rangle_{AL}$ direction is not parallel to the center-to-center vector (Figure 6c). The implication of this misalignment between atomic lattice and superlattice is a break in local 4-fold symmetry in the final superlattice, introducing disorder and contributing to the formation of local defects, *e.g.*, the absence of NC–NC epitaxial attachment seen in simulations (Figure 6d).

CONCLUSIONS

We have gained insights into NC superlattice nucleation and the role of disorder in the initial configuration with respect to subsequent epitaxial attachment. Our MD simulations suggest that square assemblies tend to form superlattices with a high degree of translational and orientational order through the formation of intermediate 2D square superstructures. For hexatic assemblies, our MD simulations demonstrate how transformation of the superlattice structure is initiated by the formation of NC dimers attached by proximal {100} facets. The transformation then propagates by dimers connecting to single NCs, or other dimers, to form larger structures that result in square domains. We confirm the existence of these "oligomers" experimentally by slowing the desorption of ligands and the subsequent oriented attachment. As the transformation propagates, dimers, trimers, and larger connected domains lose their freedom to rotate, resulting in residual misalignment and missing bridges in the final superlattice inherent to this attachment mechanism. Assemblies with initial translational structures representing ideal square and hexatic configurations with the atomic lattice aligned along the $\langle 11n \rangle_{AL}$ direction resulted in similar amounts of nearest-neighbor in-plane orientational misalignment. Purely hexatic configurations without the atomic lattice aligned along the $\langle 11n \rangle_{AL}$ direction showed a larger nearest-neighbor in-plane orientational misalignment. Introducing disorder in the form of out-of-plane misalignment of constituent NCs led to the formation of defective superlattices with missing connections for slightly tilted NCs (as observed in Figure 5). Assemblies with up to approximately 20° and 10° of initial out-of-plane rotation for square and hexatic structures, respectively, resulted in similar distributions of residual misalignment, revealing the relative robustness of the final structure to orientational disorder. In cases with more extreme levels of out-of-plane tilt, we observed attachment to take place through less favored {110} facets resulting in completely disordered structures. Hexatic configurations in which the atomic lattices were aligned along the $\langle 11n \rangle_{AL} ||\langle 11 \rangle_{SL}$ resulted in superlattices with missing epitaxial connections. Our results suggest that misalignment is inherent to the oriented attachment nucleation through dimer formation. This helps to understand the formation of defects within superlattice domains, including the absence of NC-NC epitaxial attachments and dislocations, observed by several groups. 13,46,48 This work provides insight into the coordination of irreversible oriented attachment and highlights the importance of controlling the orientation of NCs prior to

attachment, in addition to controlling ligand desorption kinetics to delay dimer formation and improve the fidelity of epitaxially connected superlattices.

METHODS

Synthesis and Characterization of Colloidal PbS and PbSe NCs. PbS NCs were prepared following a method described in detail by Hines *et al.* and Bian *et al.* 49,50 The PbSe NCs were synthesized following the procedure of Whitham *et al.* 12 scaled up to 1.2 mmol PbO. The NCs were stored inside a nitrogen glovebox. Nanocrystal size, dispersion, and concentration were measured in tetrachloroethylene (Sigma-Aldrich, 99.9%) by absorption spectroscopy using a Cary-5000 spectrometer. 51 The PbS NCs had a mean diameter of 7 nm and a polydispersity of 8% and the PbSe NCs had a mean diameter of 6.4 nm and a polydispersity of 5.6%. Oleic acid (90%), hexamethyldisilathiane (synthesis grade), 1-octadecene (90%), trioctylphosphine (97%), diphenylphosphine (98%), and selenium (99.99%) were purchased from Sigma-Aldrich. Lead oxide was purchased from Acros Organics (\geq 99.9%).

NC Superlattice Preparation and Characterization. We used the method reported by Whitham et al. 12 to form a monolayer of PbS NCs. In a glovebox, we added 20 μ L of a 0.5 μ M PbS solution in hexane to the surface of EG in a Teflon well (4 cm \times 1 cm \times 0.5 cm). The trough was immediately covered with a glass slide. After 20 min, the glass cover was removed, and 100 µL of 0.5 M EDA was gently dropcasted on EG. After 5 min, the film was transferred to a lacey carbon TEM grid coated with ultrathin carbon by the Langmuir-Schaefer method. Excess EG was rinsed with 5 mL of acetonitrile (anhydrous, 99.8%, Sigma), and the TEM grid was kept under vacuum for further solvent evaporation. The sample was characterized with cryo-STEM performed on a Thermo Fisher Scientific Titan Themis operated at 120 kV. The sample was cooled to cryogenic temperature in order to prevent buildup of contamination due to organic ligands on the NC surfaces. Scanning nanobeam electron diffraction (NBED) data were collected using an electron microscope pixel array detector (EMPAD). Each NBED frame measures 128×128 pixels. A ~ 2 nm sized probe was formed using a convergence semiangle of ~1.3

Large grain size PbSe monolayer superlattices were formed using a highly concentrated (0.26 mM) PbSe NC solution in dodecane; a small volume of the solution (0.13 μ L) was spread over a large-area trough (43 mm diameter) filled with ethylene glycol. ⁵² Samples were collected on carbon-coated TEM grids by the Langmuir—Shaefer method. The ethylene glycol was immediately soaked off using a paper tissue to prevent further transformation, and the samples were dried in vacuum. The samples were characterized in a FEI T12 TEM at 120 kV (overview image) and a FEI F20 TEM at 200 kV (atomic resolution).

Simple Molecular Reactive Force Field. The computational studies involve a traditional Molecular Dynamics (MD) approach using a reactive force field to model the interactions between species in the system. All the MD simulations were performed using Sandia's Large-Scale Atomic/Molecular Massively Parallel Simulator (LAMMPS) software. The Simple Molecular Reactive Force Field (SMRFF) pioneered by Andrejevich *et al.* is used to describe interactions between atoms. In its original implementation, it provided an accurate representation of heterogeneous metal—organic systems, which was suitable for exploring the nucleation of PbS NCs with organic ligand-covered surfaces. We use an updated version of SMRFF to calculate the total potential:

$$E_{\text{SMRFF}} = E_{\text{Morse}} S_{\text{SR}} + (E_{\text{Coulomb}} + E_{\text{LJ}}) S_{\text{LR}}$$
 (1)

This potential energy for the SMRFF potential is comprised of a combination of Morse, Coulombic, and Lennard-Jones (LJ) contributions to the energy, allowing the force field to capture both short-range (SR) and long-range (LR) pair interactions. These three individual potentials are formulated as follows:

$$E_{\text{Morse}} = D_0 [e^{-2\alpha(r - r_0)} - 2e^{-\alpha(r - r_0)}]$$
 (2)

$$E_{\text{Coulomb}} = \frac{Cq_i q_j}{r} \tag{3}$$

$$E_{\rm LJ} = 4\varepsilon \left[\left(\frac{\sigma}{r} \right)^{12} - \left(\frac{\sigma}{r} \right)^{6} \right] \tag{4}$$

where r is the interatomic distance, D_0 is the well depth (Morse), α is the width of the potential well (Morse), r_0 is the equilibrium bond distance, C is the energy-conversion constant $(1/4\pi\epsilon_0)$, q_i and q_j are the atomic charges of atoms i and j, respectively, ϵ is the depth of the potential well (LJ), and σ is the distance at which the potential is equal to 0 (LJ). The $S_{\rm SR}$ and $S_{\rm LR}$ terms in eq 1 correspond to smoothing functions to continuously transition between short-range ($S_{\rm SR}$) and long-range ($S_{\rm LR}$) regimes:

$$S_{SR} = \begin{cases} 1: r < R - D \\ \frac{1}{2} - \frac{1}{2} \sin\left(\frac{\pi}{2} \frac{r - R}{D}\right): R - D < r < R + D \\ 0: r > R + D \end{cases}$$
 (5)

$$S_{LR} = 1 - S_{SR} \tag{6}$$

Here, *R* and *D* are distance parameters delineating the transition between short- and long-range interactions. The Morse potential provides a description of covalent bonding between atoms in the NCs (covering reactive bond formation and bond breakage). A superposition of Lennard-Jones and Coulombic potentials describes other long-range interactions, such as van der Waals and dipole—dipole interactions. Geometric mixing rules were used for Lennard-Jones interactions between lead and sulfur. The parameters used to calculate the potential were reparameterized from Pb and S potentials listed in Andrejevich *et al.*³² Values for all relevant parameters can be found in the Supporting Information. The SMRFF potential was invoked for all interatomic distances <12 Å. For distances beyond this 12 Å cutoff, the computationally efficient particle—particle particle-mesh (PPPM) solver was used to calculate long-range Coulombic interactions, ensuring a smooth closure to the electrostatic forces. ⁵⁴

MD Simulation Details. Each simulated PbS NC had a diameter of 6.84 nm, similar to experimental particle sizes. In the simulation, this is equivalent to having 20 layers of atoms, with an interatomic spacing of approximately 3.6 Å per NC, corresponding to 4,848 atoms in a single NC (Figure S1). To create the NC geometries for use in MD simulations, we used Squid, an open-source codebase for file input and output. 55 To create each NC, we generated a cubic lattice of Pb and S atoms and then removed atoms from the edges to create suitable facets and arrive at the final desired shape, as shown in Figure S1. This NC was then duplicated to form an array, which was then arranged into appropriate positions and orientations to correspond to a chosen geometrical arrangement. In the 1D simulations, the NCs were initially positioned 10 Å apart and oriented with perfectly aligned {100} facets (Figure S2). For the idealized 2D simulations (Figure 2a,d), the spacing between nanocrystals is 10 Å along both the x and y axes. The remaining 2D simulations in Figure 2 with variation in initial out-of-plane rotation angles have a slightly larger spacing between NCs of 15 Å; this is to prevent NCs from overlapping when the configurations are generated. The MD simulations presented in Figure 5 all exhibit a distance of 15 Å between NCs. The configurations presented in Figure S4, aligned along the $\langle 11n \rangle_{AL}$ direction, are ~13 Å apart after they have been rotated in the plane. The final systems of 16 NCs each contain at least 77000 atoms. The final configuration for the NC assembly is read into the simulation using the Chemical Markup Language file format. All molecular visualizations are rendered using the Open Visualization Tool.

All simulations were run in a vacuum using a canonical ensemble (isothermal NVT) and a time step of 2.0 fs. Prior to this, a "minimize" command within LAMMPS is used to make sure that the configuration of atoms finds an, at least local, potential energy minimum. Experimentally, thermal annealing of NCs is conducted at $150\,^{\circ}\text{C}$, which we chose as the temperature for our simulations. The size, shape,

and atomic distribution of the NCs used in the simulation were chosen to reflect what has been observed in experiments and other sources of literature³¹ and selected in order to look at a specific orientation of adjacent NCs. For specific configurations where the NC superlattice forms and moves out of the 2D plane in which it started, these systems were run using reflective walls to slightly restrict the NCs to a 2D plane in order to mimic the experimental synthesis. Because the PPPM solver is normally reserved for systems with periodic boundaries, the *slab* option was used to remedy this issue.⁵⁷

All postprocessing calculations to analyze the MD simulation results were performed using custom-written Python code with existing functions and data types from NumPy, SciPy, and Squid. This includes calculations for determining individual NC orientations, positions, and inter-NC distances (see Supporting Information). To determine the equilibration time for in-plane orientational movement in the SL, we used two numerical criteria: the change in angle must be less than 2° between frames and the gradient must be less than 0.01. For the equilibration time for facet-to-facet distances, we used similar criteria: the change in distance must be less than 0.1 Å and the gradient must also be less than 0.01. These tolerance values were determined by visually inspecting the MD simulation frames and observing the times required for the atoms to stabilize.

ASSOCIATED CONTENT

Supporting Information

The Supporting Information is available free of charge at https://pubs.acs.org/doi/10.1021/acsnano.0c03800.

Derivation and discussion of the simple molecular reactive force field; tables including all relevant parameters used in the force field for all MD simulations; visualizations of additional MD simulation results not shown in the manuscript; relevant STEM HAADF image showing a larger field of view of the characterized region; details regarding geometric analysis of simulation results and how NC positions and orientations are calculated (PDF)

Movie S1: MD simulation results for 2 NCs separated by 10 Å as shown in Figure S2a (MP4)

Movie S2: MD simulation results for 3 NCs separated by 10 Å as shown in Figure S2b (MP4)

Movie S3: MD simulation results for 2 NCs separated by 10 Å and offset by 5 Å (MP4)

Movie S4: MD simulation results for 16 NCs in an ideal square configuration as shown in Figure 2a (MP4)

Movie S5: MD simulation results for 16 NCs in an ordered square configuration as shown in Figure 2b (MP4)

Movie S6: MD simulation results for 16 NCs in a disordered square configuration as shown in Figure 2c (MP4)

Movie S7: MD simulation results for 16 NCs in an ideal hexatic configuration as shown in Figure 2d (MP4)

Movie S8: MD simulation results for 16 NCs in an ordered hexatic configuration as shown in Figure 2e (MP4)

Movie S9: MD simulation results for 16 NCs in a disordered hexatic configuration as shown in Figure 2f (MP4)

Movie S10: MD simulation results for 16 NCs in an ideal hexatic configuration with initial in-plane alignment along the {11n} facets as shown in Figure S4a (MP4)

Movie S11: MD simulation results for 16 NCs in an ordered hexatic configuration with initial in-plane alignment along the {11n} facets as shown in Figure S4b (MP4)

Movie S12: MD simulation results for 16 NCs in a somewhat disordered hexatic configuration with variation in in-plane rotation as shown in Figure S4c (MP4)

Movie S13: MD simulation results for 9 NCs in an experimentally derived configuration as shown in Figure 3 (MP4)

AUTHOR INFORMATION

Corresponding Author

Paulette Clancy — Department of Chemical and Biomolecular Engineering, Johns Hopkins University, Baltimore, Maryland 21218, United States; orcid.org/0000-0002-0468-6420; Email: pclancy3@jhu.edu

Authors

Isaiah Y. Chen — Department of Chemical and Biomolecular Engineering, Johns Hopkins University, Baltimore, Maryland 21218, United States; ⊚ orcid.org/0000-0003-4768-9637

Jessica Cimada daSilva — Robert F. Smith School of Chemical and Biomolecular Engineering, Cornell University, Ithaca, New York 14853, United States; orcid.org/0000-0002-8108-5557

Daniel M. Balazs — Robert F. Smith School of Chemical and Biomolecular Engineering, Cornell University, Ithaca, New York 14853, United States

Michelle A. Smeaton — Department of Materials Science and Engineering, Cornell University, Ithaca, New York 14853, United States; orcid.org/0000-0001-9114-1009

Lena F. Kourkoutis — School of Applied and Engineering Physics and Kavli Institute for Nanoscale Science, Cornell University, Ithaca, New York 14853, United States; orcid.org/0000-0002-1303-1362

Tobias Hanrath — Robert F. Smith School of Chemical and Biomolecular Engineering, Cornell University, Ithaca, New York 14853, United States

Complete contact information is available at: https://pubs.acs.org/10.1021/acsnano.0c03800

Notes

The authors declare no competing financial interest.

ACKNOWLEDGMENTS

This work was primarily supported by the U.S. Department of Energy, Office of Basic Energy Sciences, under Award No. DE-SC0018026. Electron microscopy was performed in the Cornell Center for Materials Research supported by the NSF MRSEC program (DMR-1719875). The FEI Titan Themis 300 was acquired through NSF-MRI-1429155, with additional support from Cornell University, the Weill and Kavli Institutes at Cornell. J.d.S. acknowledges support from CAPES, Brazil (13159/13-5), and NSF (Award No. 1803878). M.S. acknowledges support from the NSF GRFP under Award No. DGE-1650441. I.C. and P.C. thank the Maryland Advanced Research Computing Center (MARCC), which is partially funded by the State of Maryland, for the provision of the extensive computational resources needed here. I.C. acknowledges Dr. Henry C. Herbol for his guidance with setting up the simulations.

REFERENCES

(1) Baumgardner, W. J.; Whitham, K.; Hanrath, T. Confined-But-Connected Quantum Solids *via* Controlled Ligand Displacement. *Nano Lett.* **2013**, *13*, 3225–3231.

- (2) Evers, W. H.; Schins, J. M.; Aerts, M.; Kulkarni, A.; Capiod, P.; Berthe, M.; Grandidier, B.; Delerue, C.; Van Der Zant, H. S. J.; Van Overbeek, C.; Peters, J. L.; Vanmaekelbergh, D.; Siebbeles, L. D. A. High Charge Mobility in Two-Dimensional Percolative Networks of PbSe Quantum Dots Connected by Atomic Bonds. *Nat. Commun.* 2015, 6, 1–8.
- (3) Carey, G. H.; Levina, L.; Comin, R.; Voznyy, O.; Sargent, E. H. Record Charge Carrier Diffusion Length in Colloidal Quantum Dot Solids *via* Mutual Dot-To-Dot Surface Passivation. *Adv. Mater.* **2015**, 27, 3325–3330.
- (4) Kagan, C. R.; Lifshitz, E.; Sargent, E. H.; Talapin, D. V. Building Devices from Colloidal Quantum Dots. *Science* **2016**, 353, aac5523.
- (5) Whitham, K.; Smilgies, D.-M.; Hanrath, T. Entropic, Enthalpic, and Kinetic Aspects of Interfacial Nanocrystal Superlattice Assembly and Attachment. *Chem. Mater.* **2018**, *30*, 54–63.
- (6) Boles, M. A.; Engel, M.; Talapin, D. V. Self-Assembly of Colloidal Nanocrystals: From Intricate Structures to Functional Materials. *Chem. Rev.* **2016**, *116*, 11220–11289.
- (7) Damasceno, P. F.; Engel, M.; Glotzer, S. C. Predictive Self-Assembly of Polyhedra into Complex Structures. *Science* **2012**, 337, 453–457.
- (8) Nie, Z.; Petukhova, A.; Kumacheva, E. Properties and Emerging Applications of Self-Assembled Structures Made from Inorganic Nanoparticles. *Nat. Nanotechnol.* **2010**, *5*, 15–25.
- (9) Kagan, C. R.; Murray, C. B. Charge Transport in Strongly Coupled Quantum Dot Solids. *Nat. Nanotechnol.* **2015**, *10*, 1013–1026.
- (10) Balazs, D. M.; Loi, M. A. Lead-Chalcogenide Colloidal-Quantum-Dot Solids: Novel Assembly Methods, Electronic Structure Control, and Application Prospects. *Adv. Mater.* **2018**, *30*, 1800082.
- (11) Maiti, S.; André, A.; Banerjee, R.; Hagenlocher, J.; Konovalov, O.; Schreiber, F.; Scheele, M. Monitoring Self-Assembly and Ligand Exchange of PbS Nanocrystal Superlattices at the Liquid/Air Interface in Real Time. J. Phys. Chem. Lett. 2018, 9, 739–744.
- (12) Whitham, K.; Yang, J.; Savitzky, B. H.; Kourkoutis, L. F.; Wise, F.; Hanrath, T. Charge Transport and Localization in Atomically Coherent Quantum Dot Solids. *Nat. Mater.* **2016**, *15*, 557–563.
- (13) McCray, A. R. C.; Savitzky, B. H.; Whitham, K.; Hanrath, T.; Kourkoutis, L. F. Orientational Disorder in Epitaxially Connected Quantum Dot Solids. *ACS Nano* **2019**, *13*, 11460–11468.
- (14) Sandeep, C. S. S.; Azpiroz, J. M.; Evers, W. H.; Boehme, S. C.; Moreels, I.; Kinge, S.; Siebbeles, L. D. A.; Infante, I.; Houtepen, A. J. Epitaxially Connected PbSe Quantum-Dot Films: Controlled Neck Formation and Optoelectronic Properties. *ACS Nano* **2014**, *8*, 11499–11511.
- (15) Kalesaki, E.; Evers, W. H.; Allan, G.; Vanmaekelbergh, D.; Delerue, C. Electronic Structure of Atomically Coherent Square Semiconductor Superlattices with Dimensionality below Two. *Phys. Rev. B: Condens. Matter Mater. Phys.* **2013**, 88, 115431.
- (16) Kalesaki, E.; Delerue, C.; Morais Smith, C.; Beugeling, W.; Allan, G.; Vanmaekelbergh, D. Dirac Cones, Topological Edge States, and Nontrivial Flat Bands in Two-Dimensional Semiconductors with a Honeycomb Nanogeometry. *Phys. Rev. X* **2014**, *4*, 1–12.
- (17) Alimoradi Jazi, M.; Janssen, V. A. E. C.; Evers, W. H.; Tadjine, A.; Delerue, C.; Siebbeles, L. D. A.; van der Zant, H. S. J.; Houtepen, A. J.; Vanmaekelbergh, D. Transport Properties of a Two-Dimensional PbSe Square Superstructure in an Electrolyte-Gated Transistor. *Nano Lett.* **2017**, *17*, 5238–5243.
- (18) Cölfen, H.; Mann, S. Higher-Order Organization by Mesoscale Self-Assembly and Transformation of Hybrid Nanostructures. *Angew. Chem., Int. Ed.* **2003**, 42, 2350–2365.
- (19) Colson, J. W.; Dichtel, W. R. Rationally Synthesized Two-Dimensional Polymers. *Nat. Chem.* **2013**, *5*, 453–465.
- (20) Tanoue, R.; Higuchi, R.; Enoki, N.; Miyasato, Y.; Uemura, S.; Kimizuka, N.; Stieg, A. Z.; Gimzewski, J. K.; Kunitake, M. Thermodynamically Controlled Self-Assembly of Covalent Nanoarchitectures in Aqueous Solution. *ACS Nano* **2011**, *5*, 3923–3929.
- (21) Weigelt, S.; Busse, C.; Bombis, C.; Knudsen, M. M.; Gothelf, K. V.; Lægsgaard, E.; Besenbacher, F.; Linderoth, T. R. Surface Synthesis

- of 2D Branched Polymer Nanostructures. *Angew. Chem., Int. Ed.* **2008**, 47, 4406–4410.
- (22) Libbrecht, K. G. The Physics of Snow Crystals. *Rep. Prog. Phys.* **2005**, *68*, 855–895.
- (23) Kim, B. H.; Heo, J.; Kim, S.; Reboul, C. F.; Chun, H.; Kang, D.; Bae, H.; Hyun, H.; Lim, J.; Lee, H.; Han, B.; Hyeon, T.; Alivisatos, A. P.; Ercius, P.; Elmlund, H.; Park, J. Critical Differences in 3D Atomic Structure of Individual Ligand-Protected Nanocrystals in Solution. *Science* **2020**, *368*, 60–67.
- (24) Peters, J. L.; Van Den Bos, K. H. W.; Van Aert, S.; Goris, B.; Bals, S.; Vanmaekelbergh, D. Ligand-Induced Shape Transformation of PbSe Nanocrystals. *Chem. Mater.* **2017**, *29*, 4122–4128.
- (25) Weidman, M. C.; Smilgies, D.-M.; Tisdale, W. A. Kinetics of the Self-Assembly of Nanocrystal Superlattices Measured by Real-Time *In Situ* X-Ray Scattering. *Nat. Mater.* **2016**, *15*, 775–781.
- (26) Mukharamova, N.; Lapkin, D.; Zaluzhnyy, I. A.; André, A.; Lazarev, S.; Kim, Y. Y.; Sprung, M.; Kurta, R. P.; Schreiber, F.; Vartanyants, I. A.; Scheele, M. Revealing Grain Boundaries and Defect Formation in Nanocrystal Superlattices by Nanodiffraction. *Small* **2019**, *15*, 1904954.
- (27) Geuchies, J. J.; van Overbeek, C.; Evers, W. H.; Goris, B.; de Backer, A.; Gantapara, A. P.; Rabouw, F. T.; Hilhorst, J.; Peters, J. L.; Konovalov, O.; Petukhov, A. V.; Dijkstra, M.; Siebbeles, L. D. A.; van Aert, S.; Bals, S.; Vanmaekelbergh, D. *In Situ* Study of the Formation Mechanism of Two-Dimensional Superlattices from PbSe Nanocrystals. *Nat. Mater.* **2016**, *15*, 1248–1254.
- (28) Tate, M. W.; Purohit, P.; Chamberlain, D.; Nguyen, K. X.; Hovden, R.; Chang, C. S.; Deb, P.; Turgut, E.; Heron, J. T.; Schlom, D. G.; Ralph, D. C.; Fuchs, G. D.; Shanks, K. S.; Philipp, H. T.; Muller, D. A.; Gruner, S. M. High Dynamic Range Pixel Array Detector for Scanning Transmission Electron Microscopy. *Microsc. Microanal.* **2016**, 22, 237–249.
- (29) daSilva, J. C.; Smeaton, M. A.; Dunbar, T. A.; Xu, Y.; Balazs, D. M.; Kourkoutis, L. F.; Hanrath, T. Mechanistic Insights into Superlattice Transformation at a Single Nanocrystal Level Using Nanobeam Electron Diffraction. *Nano Lett.* **2020**, *20*, 5267–5274.
- (30) Soligno, G.; Vanmaekelbergh, D. Understanding the Formation of PbSe Honeycomb Superstructures by Dynamics Simulations. *Phys. Rev. X* **2019**, *9*, 021015.
- (31) Wang, Y.; Peng, X.; Abelson, A.; Xiao, P.; Qian, C.; Yu, L.; Ophus, C.; Ercius, P.; Wang, L.-W.; Law, M.; Zheng, H. Dynamic Deformability of Individual PbSe Nanocrystals during Superlattice Phase Transitions. *Sci. Adv.* **2019**, *5*, No. eaaw5623.
- (32) Andrejevic, J.; Stevenson, J.; Clancy, P. Simple Molecular Reactive Force Field for Metal—Organic Synthesis. *J. Chem. Theory Comput.* **2016**, *12*, 825–838.
- (33) Abelson, A.; Qian, C.; Salk, T.; Luan, Z.; Fu, K.; Zheng, J.-G.; Wardini, J. L.; Law, M. Collective Topo-Epitaxy in the Self-Assembly of a 3D Quantum Dot Superlattice. *Nat. Mater.* **2020**, *19*, 49–55.
- (34) Bealing, C. R.; Baumgardner, W. J.; Choi, J. J.; Hanrath, T.; Hennig, R. G. Predicting Nanocrystal Shape through Consideration of Surface-Ligand Interactions. *ACS Nano* **2012**, *6*, 2118–2127.
- (35) Choi, J. J.; Bealing, C. R.; Bian, K.; Hughes, K. J.; Zhang, W.; Smilgies, D.-M.; Hennig, R. G.; Engstrom, J. R.; Hanrath, T. Controlling Nanocrystal Superlattice Symmetry and Shape-Anisotropic Interactions through Variable Ligand Surface Coverage. *J. Am. Chem. Soc.* 2011, 133, 3131–3138.
- (36) Li, D.; Nielsen, M. H.; Lee, J. R. I.; Frandsen, C.; Banfield, J. F.; De Yoreo, J. J. Direction-Specific Interactions Control Crystal Growth by Oriented Attachment. *Science* **2012**, *336*, 1014–1018.
- (37) Zhang, H.; De Yoreo, J. J.; Banfield, J. F. A Unified Description of Attachment-Based Crystal Growth. ACS Nano 2014, 8, 6526–6530.
- (38) Novák, J.; Banerjee, R.; Kornowski, A.; Jankowski, M.; André, A.; Weller, H.; Schreiber, F.; Scheele, M. Site-Specific Ligand Interactions Favor the Tetragonal Distortion of PbS Nanocrystal Superlattices. *ACS Appl. Mater. Interfaces* **2016**, *8*, 22526–22533.
- (39) van der Stam, W.; Rabouw, F. T.; Vonk, S. J. W.; Geuchies, J. J.; Ligthart, H.; Petukhov, A. V.; de Mello Donega, C. Oleic Acid-Induced

- Atomic Alignment of ZnS Polyhedral Nanocrystals. *Nano Lett.* **2016**, 16, 2608–2614.
- (40) Simon, P.; Rosseeva, E.; Baburin, I. A.; Liebscher, L.; Hickey, S. G.; Cardoso-Gil, R.; Eychmüller, A.; Kniep, R.; Carrillo-Cabrera, W. PbS-Organic Mesocrystals: The Relationship between Nanocrystal Orientation and Superlattice Array. *Angew. Chem., Int. Ed.* **2012**, *51*, 10776–10781.
- (41) Ondry, J. C.; Philbin, J. P.; Lostica, M.; Rabani, E.; Alivisatos, A. P. Resilient Pathways to Atomic Attachment of Quantum Dot Dimers and Artificial Solids from Faceted CdSe Quantum Dot Building Blocks. *ACS Nano* **2019**, *13*, 12322–12344.
- (42) Whitham, K.; Hanrath, T. Formation of Epitaxially Connected Quantum Dot Solids: Nucleation and Coherent Phase Transition. *J. Phys. Chem. Lett.* **2017**, *8*, 2623–2628.
- (43) Penn, R. L.; Banfield, J. F. Imperfect Oriented Attachment: Dislocation Generation in Defect-Free Nanocrystals. *Science* **1998**, *281*, 969–971.
- (44) van Huis, M. A.; Kunneman, L. T.; Overgaag, K.; Xu, Q.; Pandraud, G.; Zandbergen, H. W.; Vanmaekelbergh, D. Low-Temperature Nanocrystal Unification through Rotations and Relaxations Probed by *In Situ* Transmission Electron Microscopy. *Nano Lett.* **2008**, *8*, 3959–3963.
- (45) Jiang, Z.; Lin, X.-M.; Sprung, M.; Narayanan, S.; Wang, J. Capturing the Crystalline Phase of Two-Dimensional Nanocrystal Superlattices in Action. *Nano Lett.* **2010**, *10*, 799–803.
- (46) Ondry, J. C.; Hauwiller, M. R.; Alivisatos, A. P. Dynamics and Removal Pathway of Edge Dislocations in Imperfectly Attached PbTe Nanocrystal Pairs: Toward Design Rules for Oriented Attachment. *ACS Nano* **2018**, *12*, 3178–3189.
- (47) Centres, P. M.; Ramirez-Pastor, A. J.; Gimenez, M. C. Percolation of Defective Dimers Irreversibly Deposited on Honeycomb and Triangular Lattices. *Phys. Rev. E: Stat. Phys., Plasmas, Fluids, Relat. Interdiscip. Top.* **2018**, 98, 52121.
- (48) Walravens, W.; Solano, E.; Geenen, F.; Dendooven, J.; Gorobtsov, O.; Tadjine, A.; Mahmoud, N.; Ding, P. P.; Ruff, J. P. C.; Singer, A.; Roelkens, G.; Delerue, C.; Detavernier, C.; Hens, Z. Setting Carriers Free: Healing Faulty Interfaces Promotes Delocalization and Transport in Nanocrystal Solids. *ACS Nano* **2019**, *13*, 12774–12786.
- (49) Hines, M. A.; Scholes, G. D. Colloidal PbS Nanocrystals with Size-Tunable Near-Infrared Emission: Observation of Post-Synthesis Self-Narrowing of the Particle Size Distribution. *Adv. Mater.* **2003**, *15*, 1844–1849.
- (50) Bian, K.; Richards, B. T.; Yang, H.; Bassett, W.; Wise, F. W.; Wang, Z.; Hanrath, T. Optical Properties of PbS Nanocrystal Quantum Dots at Ambient and Elevated Pressure. *Phys. Chem. Chem. Phys.* **2014**, *16*, 8515–8520.
- (51) Moreels, I.; Lambert, K.; Smeets, D.; De Muynck, D.; Nollet, T.; Martins, J. C.; Vanhaecke, F.; Vantomme, A.; Delerue, C.; Allan, G.; Hens, Z. Size-Dependent Optical Properties of Colloidal PbS Quantum Dots. *ACS Nano* **2009**, *3*, 3023–3030.
- (52) Balazs, D. M.; Dunbar, T. A.; Smilgies, D.-M.; Hanrath, T. Coupled Dynamics of Colloidal Nanoparticle Spreading and Self-Assembly at a Fluid–Fluid Interface. *Langmuir* **2020**, *36*, 6106–6115.
- (53) Plimpton, S. Fast Parallel Algorithms for Short-Range Molecular Dynamics. *J. Comput. Phys.* **1995**, *117*, 1–19.
- (54) Hockney, R. W.; Eastwood, J. W. Computer Simulation Using Particles, 1st ed.; CRC Press: New York, 1988.
- (55) Herbol, H. C.; Stevenson, J.; Acevedo, Y.; Ruttinger, A. W.; Clancy, P. Squid, version 2.0.0a; 2019.
- (56) Stukowski, A. Visualization and Analysis of Atomistic Simulation Data with OVITO-the Open Visualization Tool. *Modell. Simul. Mater. Sci. Eng.* **2010**, *18*, 015012.
- (57) Yeh, I.-C.; Berkowitz, M. L. Ewald Summation for Systems with Slab Geometry. J. Chem. Phys. 1999, 111, 3155–3162.